Heliyon

ELSEVIER

Received:
1 August 2018
Revised:
8 October 2018
Accepted:
19 February 2019

Cite as: Larisa I. Sorokina, Egor A. Lebedev, Alexey Yu. Trifonov, Dmitry G. Gromov. Investigation of compound formation sequence in Al/Ni/…/Al/Ni multilayer system under conditions of an excessive amount of one component and its prediction using the analogy with gas system behavior. Heliyon 5 (2019) e01267. doi: 10.1016/j.heliyon.2019.e01267

Investigation of compound formation sequence in Al/Ni/…/Al/Ni multilayer system under conditions of an excessive amount of one component and its prediction using the analogy with gas system behavior

Larisa I. Sorokina [a], **Egor A. Lebedev** [a], **Alexey Yu. Trifonov** [b], **Dmitry G. Gromov** [a,c,*]

[a] *National Research University of Electronic Technology (MIET), Moscow, Zelenograd, Russia*

[b] *Scientific Research Institute of Physical Problems named after F.V. Lukin, Zelenograd, Russia*

[c] *I.M. Sechenov First Moscow State Medical University, Moscow, Russia*

[*] Corresponding author.

E-mail address: gromadima@gmail.com (D.G. Gromov).

Abstract

Interaction processes in Al/Ni/.../Al/Ni multilayer systems with an excess of one of the components are studied by of DSC, XRD and TEM methods. It is shown that the compounds formation sequence differs depending on which component is excessive. There is proposed a rule for compounds formation sequence in systems with an excess of one of the initial phases. It is based on the assumption that behaviour of two contacting solid phases system is analogical to that of a gas system: energy density change in a solid-state system is analogical to pressure change in gas system. The prediction is built on the calculation of parameter $\Delta H^0/\nu V$, where ΔH^0 and νV are enthalpy change and volume of new phase forming as a result of the reaction.

https://doi.org/10.1016/j.heliyon.2019.e01267

Keywords: Materials chemistry, Condensed matter physics, Physical chemistry, Thermodynamics

1. Introduction

Al/Ni/.../Al/Ni multilayer system has attracted the attention of researchers for a long time. This is due to its use as a composite material or application for producing rapidly solidified Al-Ni alloys with specific properties [1, 2, 3]. At the same time, it is attractive because it implements wave combustion due to self-propagating exothermic reaction between components [4, 5, 6, 7, 8]. This process is used for soldering and packaging in microelectronics [9, 10, 11, 12], as well as for joining various surfaces [13, 14]. Multilayer high-energy materials, one of which is Al/Ni/.../Al/Ni, are of considerable interest for inseparable joining of various ceramic materials [15, 16].

There are a number of publications devoted to interaction in Al-Ni system. However, the results of these studies are rather inconsistent [17, 18, 19, 20, 21, 22]. Various compositions and thickness ratios of Al/Ni layers have been studied. Different compounds formation sequences in these experiments generate different explanations for the behavior of the system. These explanations do not contradict generally accepted scientific views, but often remain unproven and hypothetical.

All this indicates the absence of a general concept of understanding processes that occur during the interaction of two contacting solid phases.

In this paper the differences in interactions in Al/Ni multilayer systems with two different layer ratios have been experimentally revealed: in one case, with an excess of Ni, in the other case with an excess of Al. Based on these data it is shown that an important role in system behavior can be played by energy density of the system, the parameter that can relate thermodynamic and kinetic features of multilayer system behavior. The aim of this work is to predict physicochemical behavior of a multilayer system depending on its composition and thermodynamic parameters, in particular, enthalpies of compound formation.

2. Experimental

The deposition of multilayer structures $(Al/Ni)_n$ on table salt substrates and oxidized Si substrates was carried out by magnetron sputtering in argon plasma in a single technological cycle. The thin film deposition facility was equipped with two DC-magnetron sputtering systems. Alternate work of magnetrons was controlled by computer in automatic mode. Using salt as a substrate is due to the ease of its dissolution in water resulting in the possibility of obtaining a multilayer foil without a substrate.

https://doi.org/10.1016/j.heliyon.2019.e01267

The studies were carried out by Differential Scanning Calorimetry (DSC), X-ray Phase Analysis (XRD), Scanning Electron Microscopy (SEM) and Transmission Electron Microscopy (TEM). Free multilayer foil was used for DSC and TEM. Multilayer film on SiO_2/Si substrate was used for XRD. The total thickness of $(Al/Ni)_n$ film was $\sim$3 μm for DSC and XRD studies, and $\sim$100 nm for TEM studies. Two compositions were studied: the first one with an excess of Al (Al:Ni ratio 4.5:1 that corresponds to Ni_2Al_9 compound composition), the second with an excess of Ni (Al:Ni ratio 1:3 that corresponds to Ni_3Al compound composition on Al-Ni phase diagram). In order to ensure these compositions the following thicknesses of Al/Ni layers were calculated: 200/50 nm for XRD samples and 20/5 nm in the case of an aluminum excess; 50/200 nm for XRD samples and 5/20 nm for TEM samples in the case of a nickel excess. Al:Ni layer thickness ratio was controlled by deposition rates of Ni and Al and a cross-section study in SEM or TEM. Al:Ni composition ratio was controlled by layer thickness ratio, EDX-analysis in SEM or EDAX-analysis in TEM.

DSC studies of solid-phase interaction processes were carried out using preliminarily calibrated DSC 204 F1 Phoenix (Netzsch-Geratebau GmbH) thermal differential calorimeter. Samples with a mass of 1−3 mg were heated in an argon atmosphere in pressed aluminum crucibles in temperature range from 25 °C to 500 °C at heating rate of 10 °C/min. The temperature of the start of solid-phase interaction was determined by the onset of heat release, which is manifested by a deviation from the linear law on DSC dependences.

After determining the temperatures of solid-phase interactions with DSC samples for XRD and TEM were annealed in vacuum at corresponding temperatures at residual gas pressure of $7 \cdot 10^{-4}$ Pa. Heating to the selected temperature was carried out at the rate of 20 °C/min. After that, the samples were held at this temperature for 40 minutes, and then cooled in a natural way.

RFA studies were performed using multifunctional X-ray diffractometer Rigaku SmartLab in symmetric reflection geometry: scanning mode was θ-2θ, the angular step - $\Delta\theta = 0.01°$, the scanning speed - 0.7°/min, the scanning range - 5−90°< and the wavelength of X-ray radiation $\lambda(CuK_{\alpha 1}) = 1.5406$ Å.

FEI Tecnai G^2 20 S-Twin electron microscope equipped with EDAX attachment for X-ray energy-dispersive microanalysis and two-beam scanning electron microscope FEI Helios NanoLab 650 i with EDX attachment were used for TEM and SEM studies, respectively.

3. Results

Fig.1a and b shows SEM images of cross sections of initial multilayer structures for DSC and XRD studies with an excess of aluminum and nickel, respectively. As can be

https://doi.org/10.1016/j.heliyon.2019.e01267

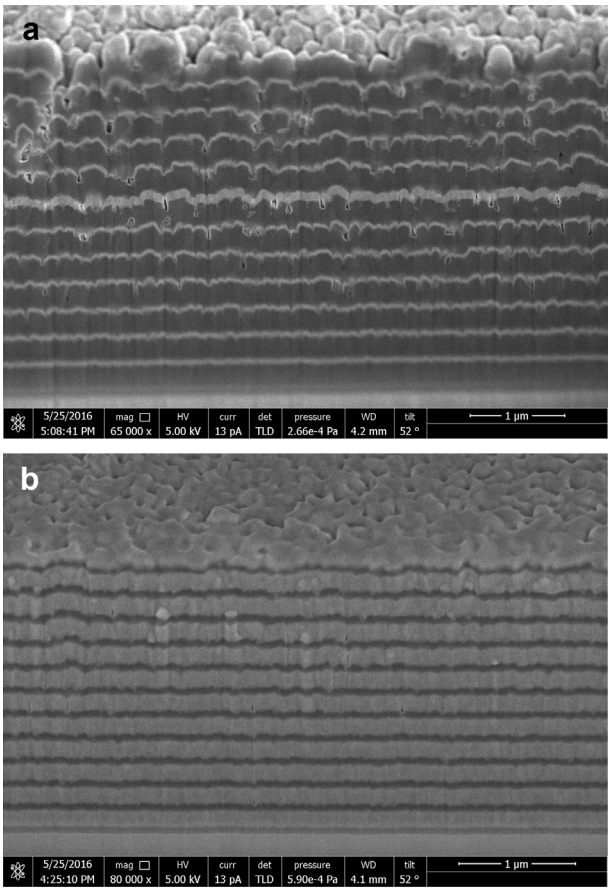

Fig. 1. SEM images of multilayer structures Al/Ni with an excess of aluminum (a) and nickel (b).

seen the total thickness of structures in both cases was ~3 μm, and the number of layer pairs was 12. The thickness of individual layers of Al and Ni was ~200 nm and ~50 nm in the case of an excess of aluminum, and ~50 nm and ~200 nm in the case of an excess of nickel, respectively. Elemental analysis showed that the atomic ratio Al:Ni in the sample with an excess of aluminum was 6:1, and the atomic ratio Ni:Al in the case of excess of nickel was 3.36:1, which is even slightly larger than expected. At the same time, the oxygen content was found to be ~10 at%.

Thermal effects in the obtained samples of multilayer films were investigated by DSC method. The results of measurements are shown in Fig. 2. For the sample enriched with aluminum (Fig. 2a) two intense peaks were recorded at 250 and 350 °C, a weak peak at 400 °C and, presumably, the shoulder of another peak at 500 °C. For the sample enriched with nickel, in the temperature range 100−500 °C three peaks are clearly visible on the heat flux curve: at 250, 350 and 450 °C (Fig. 2b).

Based on the results of DSC measurements the annealing temperatures of XRD and TEM samples were determined. These temperatures are indicated in Fig. 2(a) (aluminum excess) and (b) (nickel excess).

https://doi.org/10.1016/j.heliyon.2019.e01267

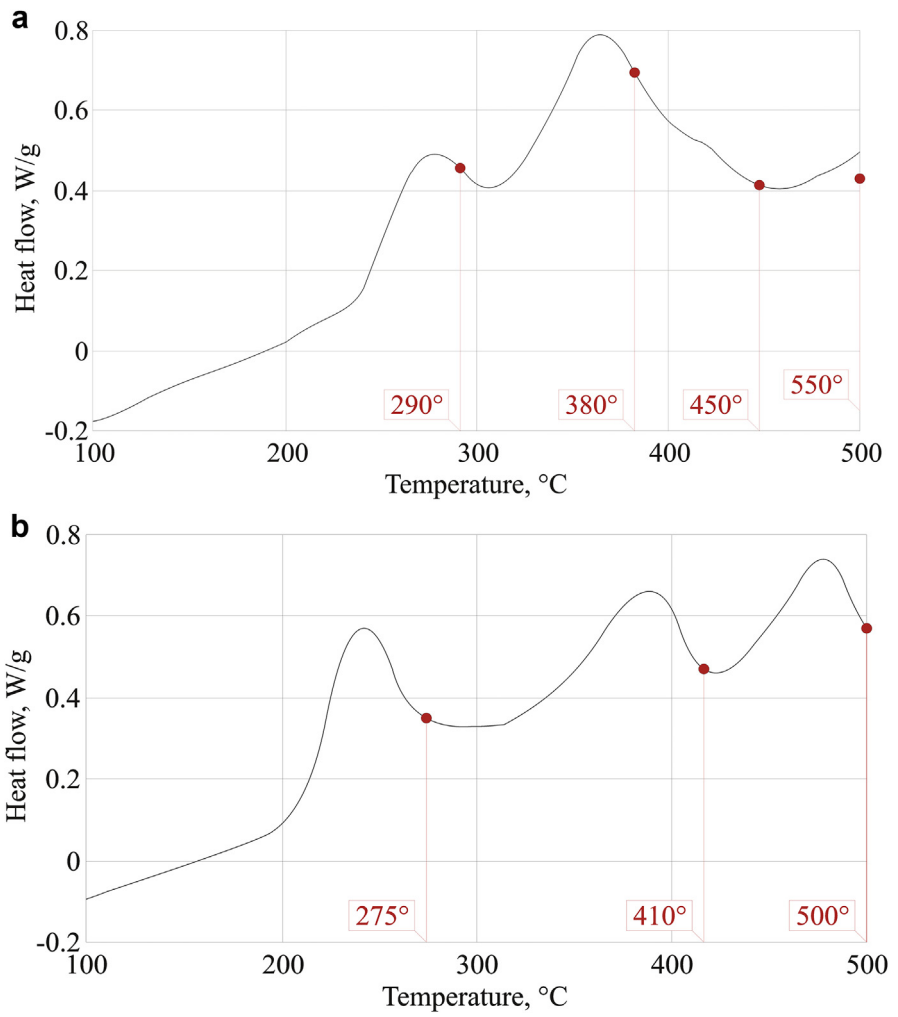

Fig. 2. The results of investigation of multilayer structures with an excess of aluminum (a) and nickel (b) by the DSC method.

3.1. The case of aluminum excess

On the X-ray diffraction pattern of the original sample only aluminum and nickel peaks were observed. Annealing at 290 °C (Fig. 3) led to the appearance of several peaks, all of which relate to NiAl compound. This allows us to conclude that it was this compound that was formed at 290 °C.

After annealing at 380 °C the X-ray diffraction pattern underwent noticeable changes (Fig. 3). Many peaks appeared. The position of 16 peaks coincides with reference data of $NiAl_3$ compound. This clearly indicates the presence of this compound in the sample. NiAl intermetallide has only 5 peaks, and only three of them are of high intensity. The peaks corresponding to these angles are present on the diffractogram. The peak at $2\theta \sim 30°$ practically coincides with $NiAl_3$ peak. However, the peaks at $2\theta \sim 45°$ and $\sim 83°$ correspond to NiAl compound and do not correspond

https://doi.org/10.1016/j.heliyon.2019.e01267

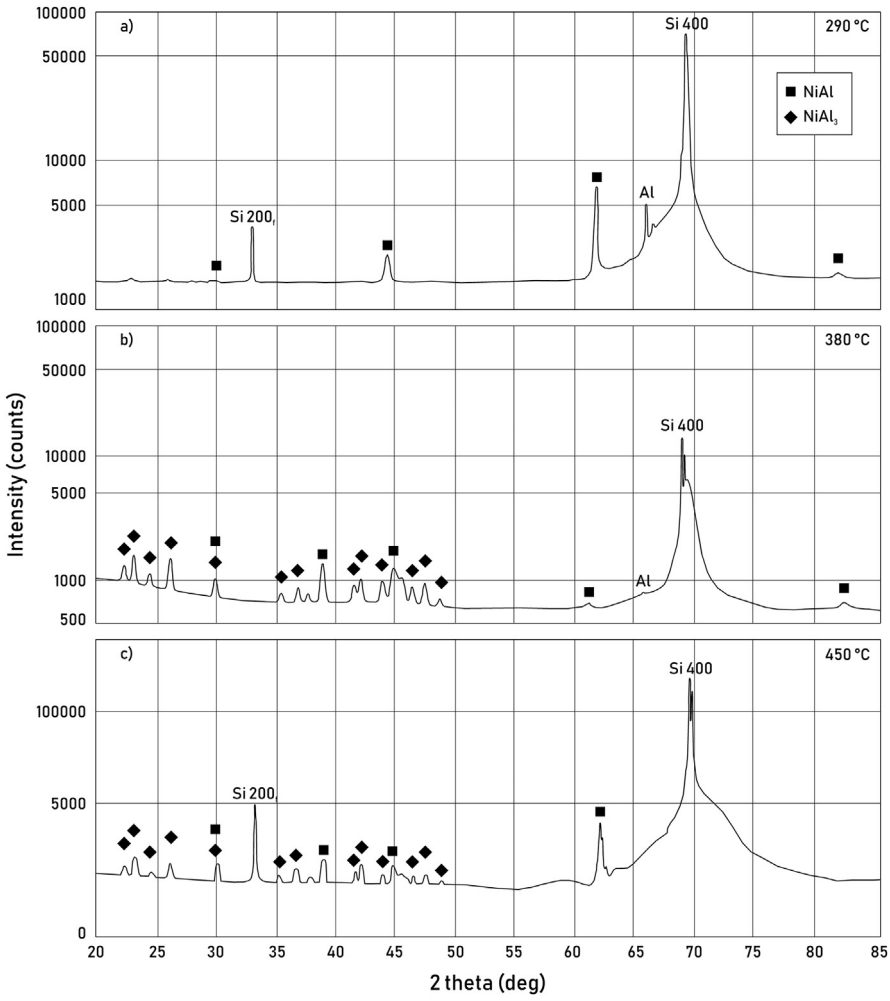

Fig. 3. X-ray diffraction patterns of the samples with an excess of aluminum annealed at different temperatures.

to $NiAl_3$. This suggests that NiAl is also present in the sample. The X-ray diffraction pattern of the sample annealed at 450 °C shows no noticeable changes in the phase composition compared to the previous annealing temperature (Fig. 3).

At the same time, TEM studies of samples of similar composition gave a different result. Fig. 4 shows TEM images of samples with aluminum excess at different annealing temperatures. Using an objective aperture due to diffraction contrast allows us to estimate dimensions of individual crystallites: dark fragments of images correspond to crystallites oriented in accordance with Bragg reflection. The figure shows that the original film is relatively homogeneous (Fig. 4a). However during the annealing process the material of the alloy is redistributed in the film: thin and thick regions are formed (Fig. 4b). And in the sample annealed at 550 °C a cluster system is formed (Fig. 4c).

https://doi.org/10.1016/j.heliyon.2019.e01267

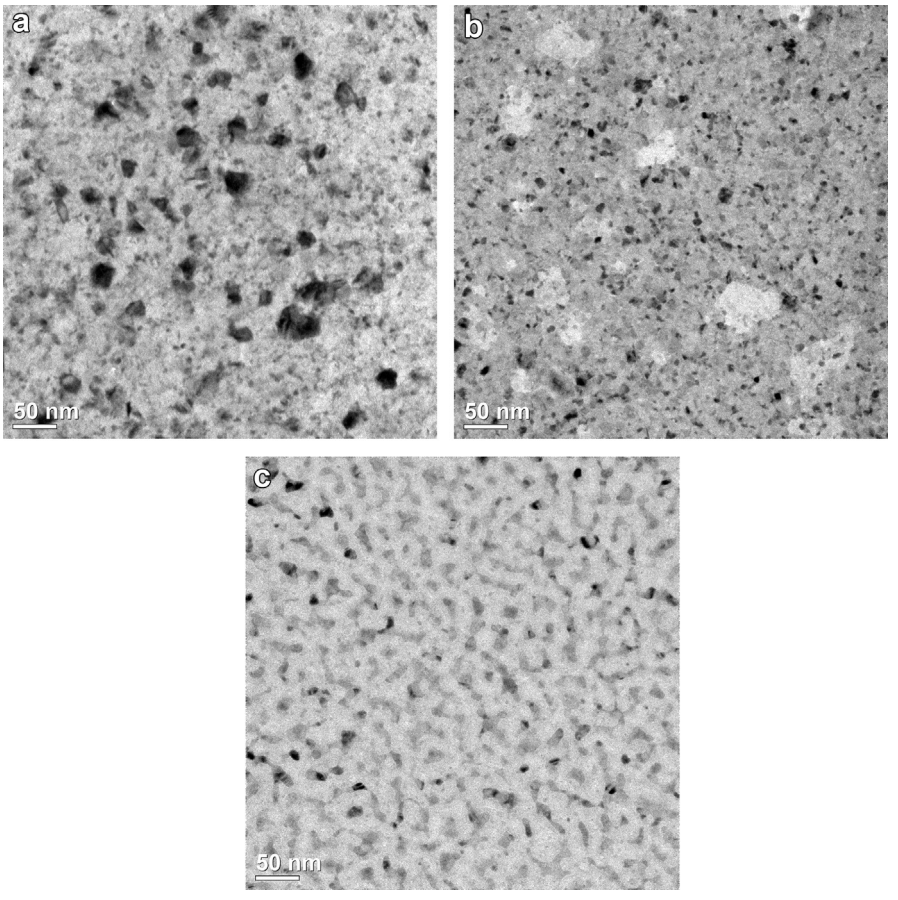

Fig. 4. TEM images of the samples with excess of aluminum at different annealing temperatures: a) original sample; b) annealing temperature 380 °C; c) annealing temperature 550 °C.

Fig. 5 shows selected-area diffraction patterns for the samples with aluminum excess. The diffraction pattern (DP) of the original sample is a combination of DP of two fcc lattices: nickel lattice with the parameter $a = 0.357$ nm and aluminum lattice with the parameter $a = 0.409$ nm. DP of nickel lattice is much weaker, since its molar fraction in the initial sample is much smaller than that of aluminum (Fig. 5a).

A set of rings characteristic of rhombohedral $NiAl_3$ lattice appears in DP after annealing at 290 °C. However the rings corresponding to hexagonal structure of Ni_2Al_3 are also present in this DP. This structure is characterized by the presence of reflections from (001) planes with a large interplanar distance $d = 0.49$ nm (Fig. 5e).

In the DP of the sample annealed at 380 °C new rings appear in comparison with the previous sample. They are typical of fcc structure with lattice constant $a = 0.355$ nm, which corresponds to a nickel lattice (Fig. 5f).

When the annealing temperature is increased to 450 °C, the rings of nickel fcc lattice in the DP become clearer, and the pattern characteristic of hexagonal structure of $NiAl_3$ disappears (Fig. 5g).

https://doi.org/10.1016/j.heliyon.2019.e01267

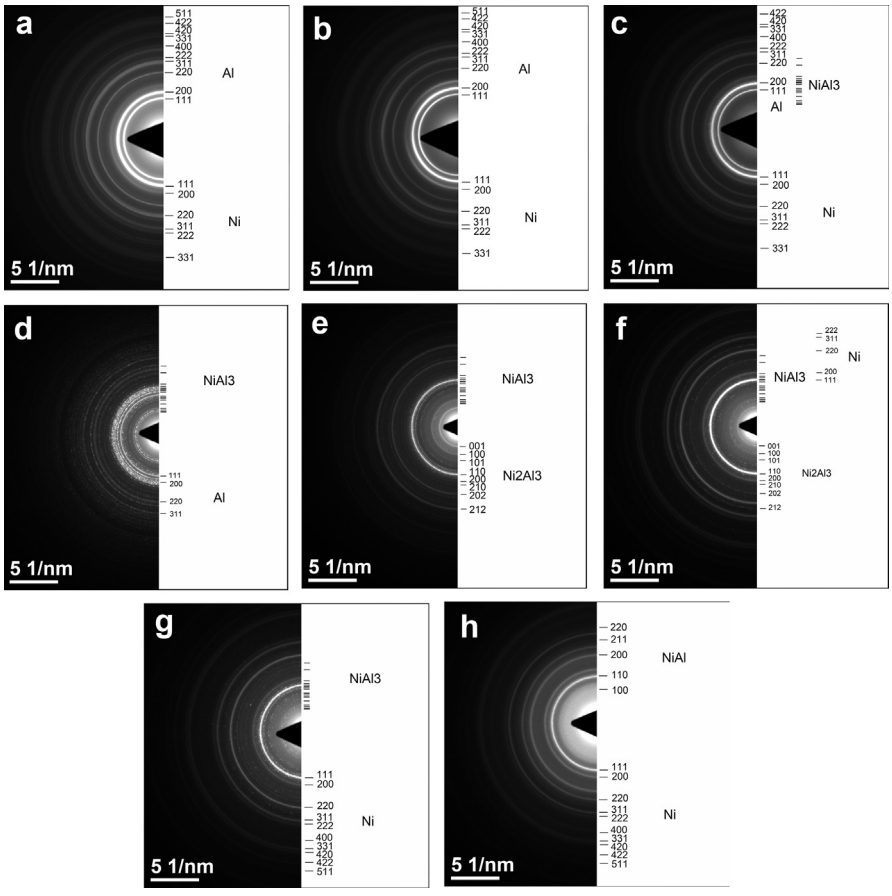

Fig. 5. Selected-area diffraction patterns for the samples with excess of aluminum: original sample (a) and the samples annealed at 100 °C (b); 150 °C (c); 200 °C (d); 290 °C (e); 380 °C (f); 450 °C (g); 550 °C (h).

In the DP of the sample annealed at maximum temperature of 550 °C there are reflexes from two crystal lattices: fcc nickel lattice and cubic lattice of cesium chloride type characteristic of NiAl compound (Fig. 5h). The latter lattice is identified by the presence of a strong ring corresponding to the (200) planes. This ring is absent in the DP of nickel fcc lattice. In addition, a halo appears in the DP. Considering that we are dealing with the case of aluminum excess, appearance of nickel and a compound slightly enriched in aluminum seems rather strange. Furthermore, it is not clear what happens to the released aluminum.

To clarify this situation, X-ray energy-dispersive spectra of this sample were obtained. The results of these measurements are presented in Fig. 6. It can be seen that outside clusters there is practically no nickel, but there is a strong peak of aluminum. At the same time, peaks of both elements of the investigated alloy are present in the clusters (Fig. 6b). The survey spectrum (Fig. 6a) gives some average elemental composition. A large peak of oxygen is present in the spectra. This suggests that when heated to relatively high temperatures, aluminum being a more

https://doi.org/10.1016/j.heliyon.2019.e01267

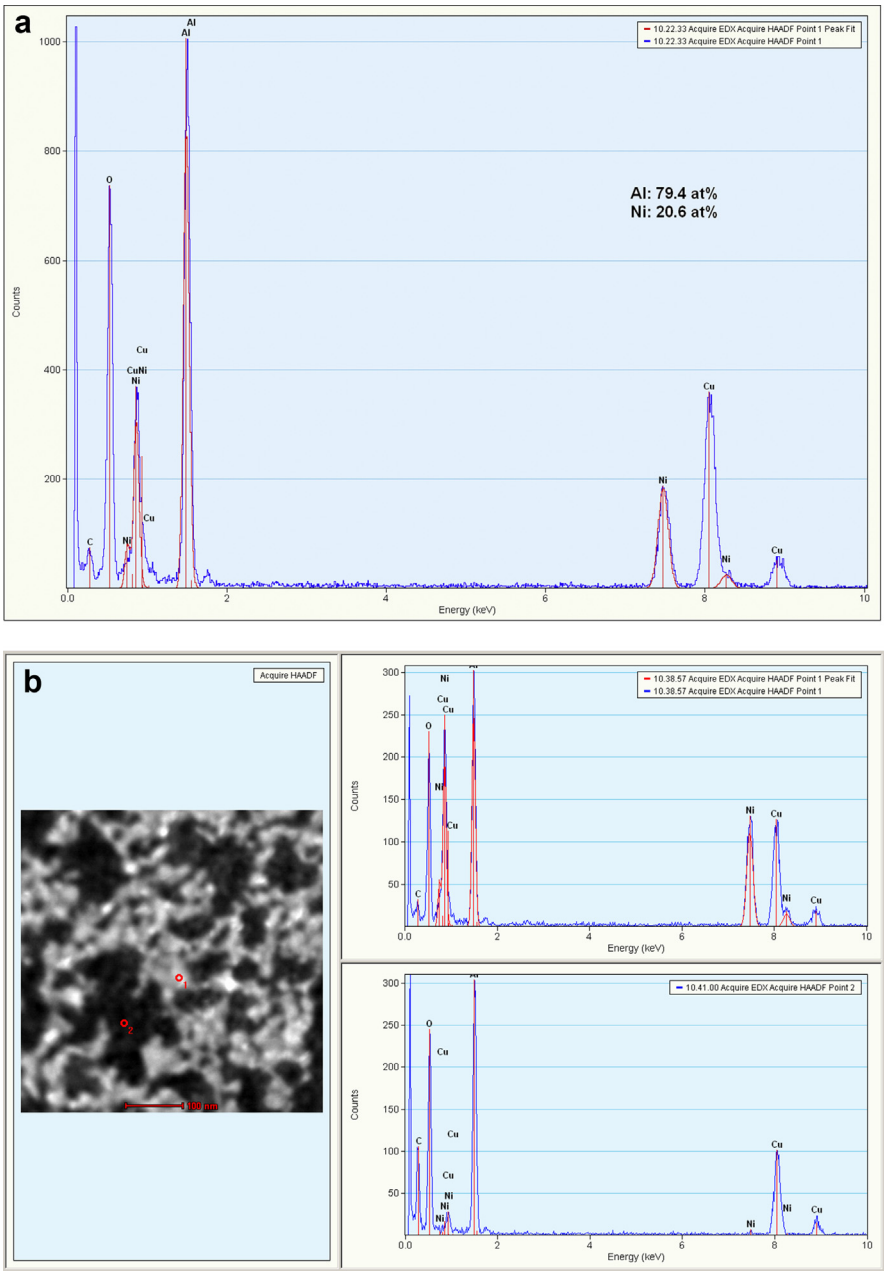

Fig. 6. X-ray energy-dispersive spectra of the sample with an excess of aluminum annealed at 550 °C: a) survey spectrum; b) local spectra in points 1 and 2 shown in STEM image.

active element begins to react with residual oxygen present in the chamber. As a result aluminum excess is removed from the alloy and a film of amorphous aluminum oxide is formed. The same fact can also explain the inconsistency of elemental composition of the observed polycrystalline compounds and the composition of the initial sample.

https://doi.org/10.1016/j.heliyon.2019.e01267

The difference between the results of TEM studies and XRD may be due to the fact that TEM samples have thinner layers, and interaction in them can go more easily. Therefore, we performed additional annealing at lower temperatures of 100, 150, and 200 °C.

The DP of the sample annealed at 100 °C (Fig. 5b) practically does not differ from the initial sample: it also contains fcc lattices of nickel and aluminum.

When the annealing temperature is increased to 150 °C (Fig. 5c), traces of several, the brightest, rings of $NiAl_3$ compound with rhombohedral crystal lattice are added to the diffraction pattern.

In the sample annealed at 200 °C (Fig. 5d) the DP changes radically: it is clearly dominated by numerous rings of rhombohedral lattice of $NiAl_3$. Against this background only a few rings of fcc lattice of aluminum can be distinguished.

Thus in the case of aluminum excess XRD studies show that NiAl compound is formed first, and then comes the formation of $NiAl_3$. At the same time, a detailed TEM study demonstrates that $NiAl_3$ compound maximally enriched with aluminum is immediately formed at temperature of 150 °C.

3.2. The case of nickel excess

On the X-ray diffraction pattern of the original sample (Fig. 7) only aluminum and nickel peaks are observed as well as in the case of aluminum excess. However annealing at 275 °C leads to the appearance of a set of peaks (Fig. 7), which significantly differs from the case of aluminum excess (Fig. 7). Although the annealing temperatures were close enough. All characteristic peaks of NiAl phase are observed. Nickel peaks are also present, which indicates that only part of it interacted with aluminum. The weak intensity of peaks corresponding to $NiAl_3$ phase indicates that its amount is extremely small. The diffractogram of the sample annealed at 410 °C is significantly different from the previous one: the peaks corresponding to $NiAl_3$ compound completely disappeared; peaks of NiAl remained, and new peaks strictly corresponding to Ni_3Al intermetallide appeared. Annealing at 500 °C did not lead to a noticeable change.

Fig. 8 shows TEM images of the samples with a nickel excess at different annealing temperatures. Diffraction contrast allows us to estimate the size of crystallites. The sample annealed at 550 °C is somewhat different in appearance from others. The crystallite size in this sample is slightly larger.

Fig. 9 shows selected-area diffraction patterns for NiAl samples with nickel excess. The DP of the initial sample not subjected to annealing is a combination of two patterns: fcc lattice of nickel with the parameter $a = 0.355$ nm and fcc lattice of aluminum with the parameter $a = 0.410$ nm. The DP of aluminum lattice is much

https://doi.org/10.1016/j.heliyon.2019.e01267

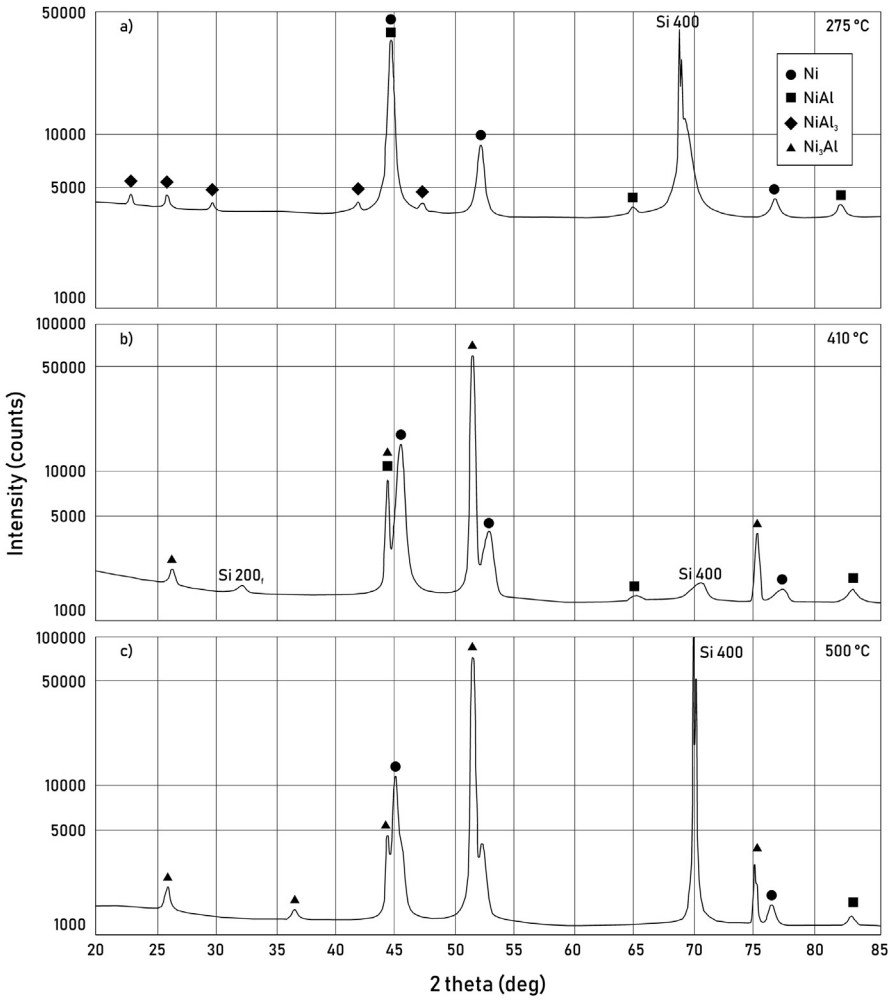

Fig. 7. X-ray diffraction patterns of the samples with an excess of nickel annealed at different temperatures.

weaker, since its molar fraction in the initial sample is much smaller than that of nickel (Fig. 9a).

After annealing at temperature of 275 °C the rings corresponding to fcc lattice of aluminum disappear in the DC, and very weak rings corresponding to cubic lattice of NiAl (cesium chloride type) are added to the rings of fcc lattice of Ni (Fig. 9b).

The DP of the sample annealed at 410 °C (Fig. 9c) is a superposition of patterns corresponding to Ni_3Al compound and fcc lattice of nickel. Crystal structure of Ni_3Al relates to Cu_3Al type and represents fcc structure with superlattice. The lattice parameters of Ni and Ni_3Al are very close. Therefore the corresponding rings of the DP acquire some blurring, which becomes especially noticeable as their radius increases. Due to the presence of superlattice the DP of Ni_3Al includes so-called "chemically sensitive" reflexes, which are forbidden in the classical fcc structure. In Fig. 3 c only the rings corresponding to these reflexes of Ni_3Al are marked.

https://doi.org/10.1016/j.heliyon.2019.e01267

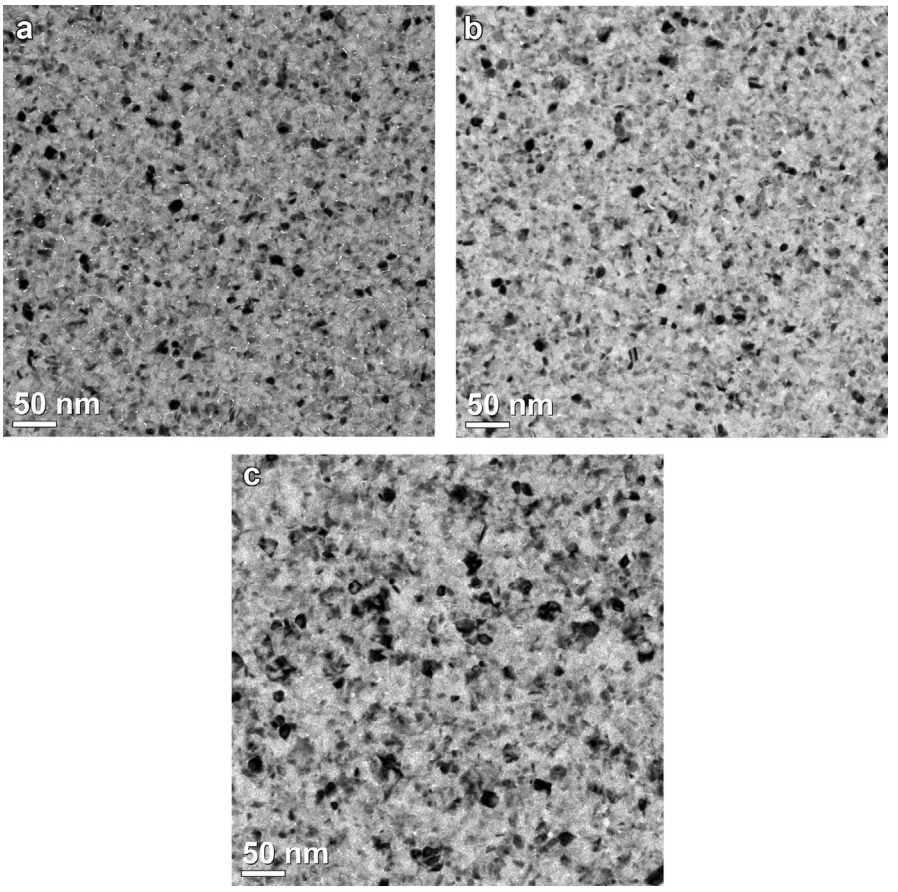

Fig. 8. TEM images of the samples with excess of nickel at different annealing temperatures: a) original sample; b) annealing temperature 275 °C; c) annealing temperature 550 °C.

The DP of the sample annealed at 550 °C (Fig. 9d) practically does not differ from the previous one (Fig. 9e).

Thus in the case of nickel excess both XRD and TEM studies actually show the same sequence of compound formation: first NiAl compound is formed, and then Ni_3Al is formed.

4. Discussion

The results presented in the study show that the sequences of compounds formed in $(Al/Ni)_n$ multilayer structures enriched in Al and Ni turn out to be different. Moreover, XRD on thick films and TEM on thinner films show different sequences. Thus there can be distinguished two extreme cases.

The first extreme case deals with a contact through one interphase boundary of two phases: Al phase and Ni phase, one of which is in large excess with respect to the other. In this case because of diffusion limitations the system moves through a

https://doi.org/10.1016/j.heliyon.2019.e01267

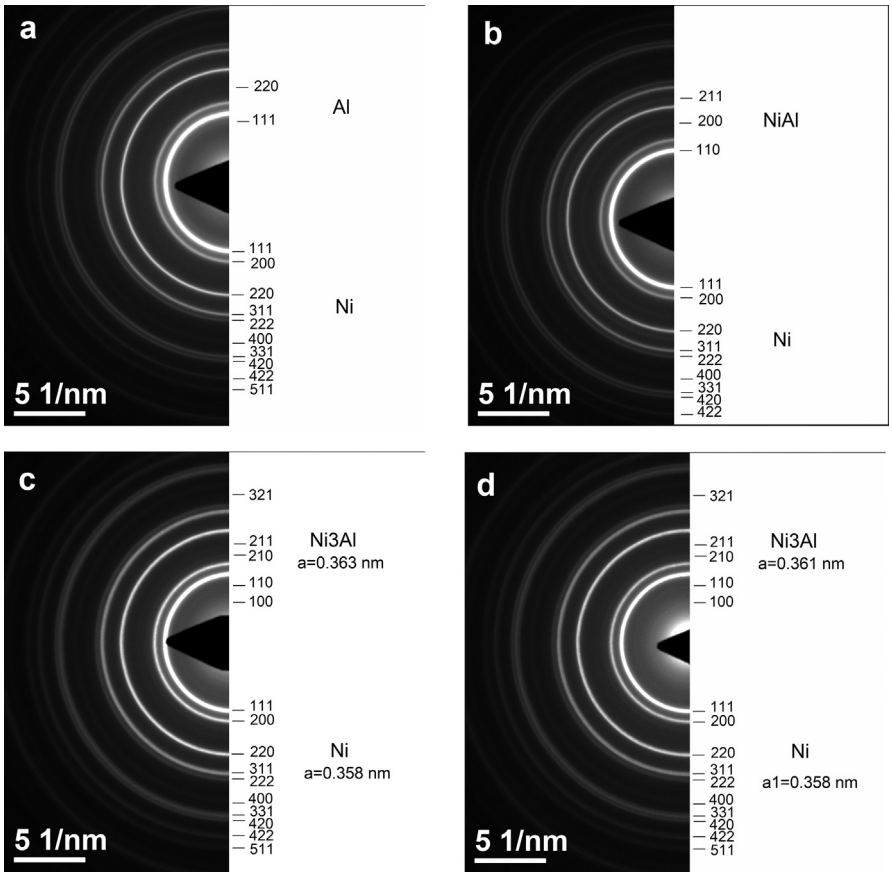

Fig. 9. Selected-area diffraction patterns for the samples with excess of nickel: original sample (a) and the samples annealed at 275 °C (b); 410 °C (c); 550 °C (d).

sequence of compounds being formed. The last in the sequence is the compound maximally enriched with the excess component. This case has been studied quite well in systems that form metal silicides, because they are traditionally used in VLSI technology [23]. The typical condition of their formation is a large excess of silicon in comparison with metal. In particular, it is shown that in Ni-Si system Ni_2Si compound, the most stable in this system, is always formed first. However after this in the case of a Si excess NiSi and $NiSi_2$ are sequentially formed from it, and in the case of a Ni excess Ni_5Si_2 and Ni_3Si are formed. The sequence of compounds formation in metal/silicon systems with one component excess is well justified from the standpoint of the theory of classical nucleation [24]. It is characteristic that the driving forces of each subsequent solid-phase chemical reaction of the compound formation decrease compared to the previous one as the concentration of silicon in these phases increases. (In the system under consideration, we can also see this trend in Table 2 below). Calculating enthalpy of the reactions show that if any compound was formed first, the enthalpies of all subsequent reactions of formation from it of other compounds more enriched with the excess component (if any) are

https://doi.org/10.1016/j.heliyon.2019.e01267

negative. This indicates that these reactions are spontaneous and can proceed. Another question is, which one of them will prevail?

The second extreme case is a multilayer structure with a large number of interfaces and, importantly, a very small thickness of layers. In this case there are no diffusion restrictions, and a compound corresponding to the quantitative ratio of the system components is formed first.

It should be noted that depending on their total thickness, the ratio of layer thicknesses and the number of multilayer systems very often could represent an intermediate case between these two extreme cases. Diffusion limitations then are present partially. And this is the most difficult case to predict. In this context the results of in-situ studies presented in works [25, 26] are also illustrative. In both cases thin multilayer samples suitable for TEM with Al:Ni ratio of 1:1 and layer thicknesses of $\sim$25 nm were examined. This is also close to the second extreme case mentioned above. However the samples had fundamental differences. In one case there was a planar structure with extended Al/Ni interfaces [25], and in the other there was a cross section with many short Al/Ni interfaces [26]. It turns out that they behave differently: in one work the formation of NiAl compound was immediately observed, and in the other NiAl formation was first observed after the formation of $NiAl_3$ and Ni_2Al_3 compounds.

Obviously, low-temperature formation of $NiAl_3$compound $NiAl_3$ observed by TEM for the case of aluminum excess is close to the second extreme case. It is significant that this compound is formed despite the fact that it is incongruent-melting and is the most unstable in Al-Ni system. It is also characteristic that at a higher temperature it disintegrates in strict accordance with the phase diagram: Ni_2Al_3 incongruent-melting compound appears and also disintegrates with increasing the temperature, i.e. with the formation of NiAl compound which is the most stable for this system.

We propose to explain the dissimilar behavior of multilayer systems with an explicit excess of one or the other component by analogy with the behavior of model gas systems. The basis for the analogy between the behavior of gas system and solid-phase system is the following reasoning. Consider the well-known expression:

$$H = U + pV$$

If we divide both its parts by volume V, then we get:

$$\frac{h}{V} = \frac{U}{V} + p.$$

Values of different nature cannot be summed up, and hence from this expression it follows that the density of internal energy $u = U/V$ is equivalent to the force acting per unit area, that is, pressure. Thus we assume that the behavior of

https://doi.org/10.1016/j.heliyon.2019.e01267

solid-phase system can be estimated from the change in energy density, in the same way as the behavior of gas system can be estimated from the change in pressure in the system.

The proposed model for interaction of two contacting solid phases is based on the use of parameter $\Delta_r H_{298}/\nu V$, where $\Delta_r H_{298}$ (kJ/mol) is the enthalpy change due to the chemical reaction of formation of a new compound; V is the molar volume of the new compound formed as a result of the reaction; ν is the number of moles of the new compound. In addition, we assume that $\Delta_r H_{298}/\nu V$ characterizes the change in energy density (enthalpy density h and density of internal energy u).

The scheme of the model gas system is shown in Fig. 10. N vessels through the valves are connected to a vessel of volume V_0. All vessels contain the same gas. At the initial moment the valves are closed and the gas pressures in all the vessels are known:

$$p_i(t=0)=p_{i0},\ i=0,\ 1,\ 2,\ \ldots,\ N. \tag{1}$$

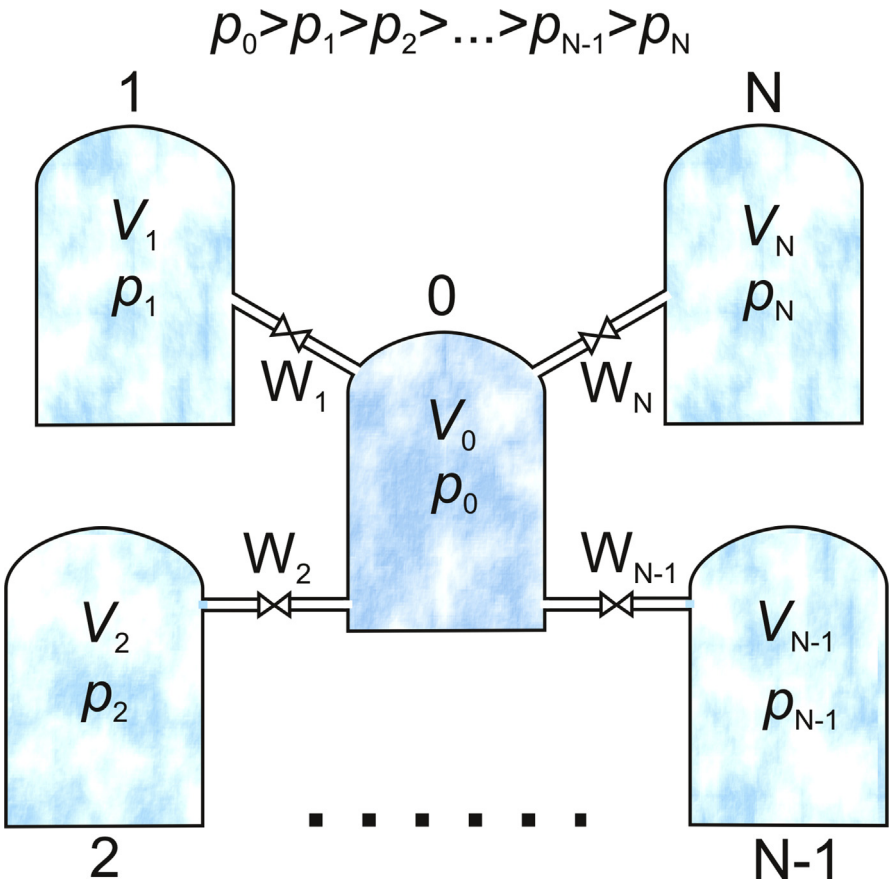

Fig. 10. The scheme of the model gas system.

https://doi.org/10.1016/j.heliyon.2019.e01267

We assume that at the initial moment all the valves are open. Let us determine the dependences of gas pressures in all the vessels on time.

Assuming that the gas flow through the pipeline is proportional to the pressure difference in the respective vessels, and the pressure at constant temperature is proportional to the concentration, we obtain the following equations for the pressure change rate in the vessels:

$$\frac{dp_i}{dt} = \frac{1}{W_i V_i} \cdot (p_0 - p_i),\ i > 0;\ \frac{dp_0}{dt} = \frac{1}{V_0} \cdot \sum_{i=1}^{N} \frac{1}{W_i} \cdot (p_i - p_0), \tag{2}$$

where W_i is the resistance of pipe i to the gas flow. This quantity depends on length and cross-section of the pipe and is analogous to electrical resistance. Thus, the behavior of the system is described by a system of homogeneous linear differential equations with constant coefficients:

$$\begin{pmatrix} \frac{dp_1}{dt} \\ \dots \\ \frac{dp_N}{dt} \\ \frac{dp_0}{dt} \end{pmatrix} = \begin{pmatrix} -\frac{1}{W_1 V_1} & \dots & 0 & \frac{1}{W_1 V_1} \\ \dots & \dots & \dots & \dots \\ 0 & \dots & -\frac{1}{W_N V_N} & \frac{1}{W_N V_N} \\ \frac{1}{W_1 V_0} & \dots & \frac{1}{W_N V_0} & -\frac{1}{V_0} \sum_{i=1}^{N} \frac{1}{W_i} \end{pmatrix} \begin{pmatrix} p_1 \\ \dots \\ p_N \\ p_0 \end{pmatrix} \tag{3}$$

Its general solution is:

$$p = \sum_{i=1}^{N} C_i h_i e^{\lambda_i t} + C_0; \tag{4}$$

where p is the column of pressures; C_i are constants determined from the initial conditions (1); λ_i are eigenvalues, and h_i are the corresponding eigenvectors of the matrix of the system of Eq. (3). All eigenvalues λ_i are negative, and the inverse values of their modules are the relaxation times of the corresponding exponentials. The constant C_0 is the average pressure that will be established in all vessels as $t \to \infty$:

$$C_0 = \frac{\sum_{i=0}^{N} n_i V_i}{\sum_{i=0}^{N} V_i}; \tag{5}$$

Thus the process of pressure equalization is a combination of N exponential processes with different relaxation times. As a result the curves of dependences $p_i(t)$ can turn out to be quite sophisticated.

In particular, the derivative of this function p_i' can change sign. On the one hand, p_i' is proportional to the pressure difference in reservoirs 0 and i and is inversely

https://doi.org/10.1016/j.heliyon.2019.e01267

proportional to the resistance of pipeline *i*. On the other hand, p_i' is a flow from the 0th reservoir to reservoir *i*, and changing its sign indicates a change in the direction of this flow. Actually, at the initial time the largest gas flow is directed into the reservoir with minimum resistance of the corresponding pipeline. However after a while it weakens and can be directed out of it, because the pressure difference between the central reservoir and other *i*-th reservoir is still large.

Let us draw an analogy between the considered gas model and the process of interaction of two contacting solid phases. We assume that the change in the energy density *u* or *h* of the system during the chemical reaction of formation of a new compound at the boundary of two contacting solid phases occurs according to a law that is similar to the pressure change in gas system. Central reservoir 0 connected to *N* reservoirs by closed pipelines with various resistances is similar to the initial state of two contacting phases. Reservoirs 2, 3 ... *N* are analogous to compounds that can form in the system. Resistance of the pipeline *W* is analogous to the kinetic limitations - the processes of diffusion and nucleation.

The initial time when two solid phases are brought into contact corresponds to simultaneous opening of all valves and the emergence of gas flows from reservoir 0 to all the other reservoirs. This means that simultaneously the processes of nucleation of all compounds having negative ΔH_f^0 will begin. However according to the gas example the largest matter flow will be directed to the formation of that compound, the nucleation and growth process of which is accompanied by the fastest decrease of energy density *u* or *h* in the system, which indicates the maximum process speed. Moreover, if due to the formation of rapidly growing new phase *u* or *h* in the system would be less than the values corresponding to the formation of other new phases, then according to the gas example a flow of matter from these phases will arise. In other words, if the density of internal energy of the system during nucleation and growth of any other phase changes very slowly, then the emerging nuclei of this phase will begin to dissolve. Obviously, if the processes of formation of several compounds proceed with close rates of change in the energy density in the system, then such compounds will grow simultaneously (parallel reactions). The growth of the compound (or compounds) with fast dynamics will continue until one of the initial contacting phases is completely consumed. If the excess of the other contacting phase remains in this case, then we again have two contacting macrophases, one of which is now a formed compound (or mixture of compounds). As a result the process of formation of the compound (or compounds) of the excess initial phase enriched with the component will follow the same principle. In turn, the change of contacting phases to more enriched ones will occur until a homogeneous or microheterogeneous system arises (consecutive reactions).

Thus, it is possible to formulate a *rule for compounds formation sequence in the interaction of two contacting solid phases*:

https://doi.org/10.1016/j.heliyon.2019.e01267

If the system has an excess of one of the initial phases, and it is possible to form multiple compounds in it, then the system proceeds according to those compounds formation sequence, which most rapidly reduces the density of internal energy in the system.

In solid-phase system it is impossible to determine the variation of u at any time. However, if we consider all possible sequences of chemical reactions of compounds formation in the system and calculate values of $\Delta H^0/\nu V$ of these reactions, we can determine the variation of u with respect to the initial state as a result of each subsequent reaction in the sequence. The value of u can be represented as a function of mole fraction x of the excess component in the respective compounds. Since the mole fraction of the excess component varies monotonically with time, its change can be considered as an analog of time in the example with the gas system. Therefore, taking into account expression (4) the calculated points with some approximation can be approximated by the following function:

$$u = a \cdot \exp(-bx) + \exp\left(-cx^k\right) + d, \tag{6}$$

The result is a set of curves $u(x)$, characterizing integral change in the energy density of the system of two contacting phases as a function of the excess component mole fraction in the initial phase when the system realizes various paths of motion to the equilibrium state. Obviously, in the case of an infinitely large amount of a component of one of the initial phases compared to the component of the second initial phase all paths must lead to the same equilibrium state-the infinitely dilute solution of the second phase component in the first component. This state is characterized by a certain level of internal pressure, so that all curves $u(x)$ obtained in the approximation process must converge to one point at $x = 1$. The most preferred path is determined in accordance with the rule justified above.

The publications on thermodynamic and physical properties of the Al-Ni system were analyzed. Table 1 shows the initial data found, which we need to calculate. As can be seen the data of various authors on the enthalpy of formation of Al-Ni system compounds often differ significantly. In our calculations, we did not take into account the values that were clearly falling out, and for the rest we obtained an average value.

At the first stage we consider all possible chemical reactions in the system and define their $\Delta_r H_{298}$ and $\Delta_r H_{298}/\nu V$. The results of this stage for Ni-Si system are presented in Table 2. On the basis of the calculated data presented in Table 2 and according to the above stated rule of the sequence of compounds formation we shall compose the main sequences of motion of Ni-Al system to the equilibrium state for two cases: an infinite excess of aluminum and an infinite excess of nickel.

https://doi.org/10.1016/j.heliyon.2019.e01267

Table 1. Physico-chemical data of the Ni-Al system.

Compound	$-\Delta H^0_{f298}$, kJ/g×at.	Density, g/cm^3	Molar volume V, cm^3	Molar volume V, cm^3/g×at.	$-\Delta H^0_{f298}$/V kJ/cm^3
Al	0	2710 [27] 2710 [28] 2700 [29]	9.96	9.96	0
Ni_2Al_9	28.1 [30]	–	99.77	9.07	3.09
$NiAl_3$	42.1 [27] 22.2 [32] 37.7 [34] 36.0 [35] 38.0 [36] 36.2 [37] 37.7 [38]	4100 [27] 3930 [31] 3980 [33]	34.91	8.73	4.82 2.54 4.32 4.12 4.35 4.15 4.32
Ni_2Al_3	64.5 [27] 75.5 [39] 62.7 [40] 61.8 [32] 58.9 [41] 56.5 [34] 57.0 [36]	4900 [27]	40.47	8.09	7.97 9.33 7.75 7.64 7.28 6.98 7.05
Ni_3Al_4	65.9 [27]	5220 [27]	54.40	7.77	8.48
NiAl	69.5 [27] 66.8 [39] 77.3 [42] 71.4 [43] 67.5 [44] 71.4 [41] 71.0 [45] 80.0 [46] 76.0 [47] 71.0 [48] 76.0 [32] 79.0 [49] 63.0 [50] 66.0 [51] 66.4 [52] 58.3 [53] 62.0 [54] 61.8 [55] 66.5 [56]	6040 [27] 5880 [42] 5920 [57]	14.40	7.20	9.65 9.28 10.74 9.92 9.38 9.92 9.86 11.11 10.56 9.86 10.56 10.97 8.75 9.17 9.22 8.10 9.17 8.61 9.24
Ni_5Al_3	61.5 [27] 56.0 [40]	6730 [27]	55.63	6.95	8.85 7.78
Ni_3Al	47.5 [27] 44.4 [40] 48.2 [32] 47.3 [44] 45.7 [42] 38.6 [41] 37.0 [35] 41.0 [36] 41.4 [51] 40.5 [46]	7500 [27] 7450 [42] 7440 [58] 7440 [59]	27.22	6.81	6.98 6.52 7.08 6.95 6.71 5.67 5.43 6.02 6.09 5.95
Ni	0	8870 [27] 8880 [28] 8910 [29]	6.60	6.60	0

https://doi.org/10.1016/j.heliyon.2019.e01267

Table 2. Potential chemical reactions in the Ni-Al system.

№	Reaction	$\Delta_r H^0_{298}$, kJ/mol	$\Delta_r H^0_{298}/\nu V$, kJ/cm^3
1	$2Ni + 9Al \rightarrow Ni_2Al_9$	−308.0	−3.09
2	$Ni + 3Al \rightarrow NiAl_3$	−144.0	−4.12
3	$2Ni + 3Al \rightarrow Ni_2Al_3$	−313.5	−7.75
4	$3Ni + 4Al \rightarrow Ni_3Al_4$	−461.3	−8.48
5	$Ni + Al \rightarrow NiAl$	−139.0	−9.55
6	$5Ni + 3Al \rightarrow Ni_5Al_3$	−492.0	−8.85
7	$3Ni + Al \rightarrow Ni_3Al$	−177.6	−6.52
8	$Ni_2Al_9 + Ni \rightarrow 3NiAl_3$	−124.0	−1.18
9	$Ni_2Al_9 + 4Ni \rightarrow 3Ni_2Al_3$	−632.5	−5.21
10	$4Ni_2Al_9 + 19Ni \rightarrow 9Ni_3Al_4$	−2919.7	−5.96
11	$Ni_2Al_9 + 7Ni \rightarrow 9NiAl$	−943.0	−7.28
12	$Ni_2Al_9 + 13Ni \rightarrow 3Ni_5Al_3$	−1168.0	−7.00
13	$Ni_2Al_9 + 25Ni \rightarrow 9Ni_3Al$	−1290.4	−5.26
14	$NiAl_3 + Ni \rightarrow Ni_2Al_3$	−169.5	−4.19
15	$4NiAl_3 + 5Ni \rightarrow 3Ni_3Al_4$	−807.9	−4.95
16	$NiAl_3 + 2Ni \rightarrow 3NiAl$	−273.0	−6.32
17	$NiAl_3 + 4Ni \rightarrow Ni_5Al_3$	−348.0	−6.26
18	$NiAl_3 + 8Ni \rightarrow 3Ni_3Al$	−388.8	−4.76
19	$4Ni_2Al_3 + Ni \rightarrow 3Ni_3Al_4$	−129.9	−0.80
20	$Ni_2Al_3 + Ni \rightarrow 3NiAl$	−103.5	−2.40
21	$Ni_2Al_3 + 3Ni \rightarrow Ni_5Al_3$	−178.5	−3.21
22	$Ni_2Al_3 + 7Ni \rightarrow 3Ni_3Al$	−219.3	−2.68
23	$Ni_3Al_4 + Ni \rightarrow 4NiAl$	−94.7	−1.64
24	$3Ni_3Al_4 + 11Ni \rightarrow 4Ni_5Al_3$	−584.1	−2.63
25	$Ni_3Al_4 + 9Ni \rightarrow 4Ni_3Al$	−249.1	−2.29
26	$3NiAl + 2Ni \rightarrow Ni_5Al_3$	−75.0	−1.35
27	$NiAl + 2Ni \rightarrow Ni_3Al$	−38.6	−1.42
28	$Ni_5Al_3 + 4Ni \rightarrow 3Ni_3Al$	−40.8	−0.50
29	$5Ni_3Al + 4Al \rightarrow 3Ni_5Al_3$	−588.0	−3.53
30	$Ni_3Al + 2Al \rightarrow 3NiAl$	−239.4	−5.54
31	$Ni_3Al + 3Al \rightarrow Ni_3Al_4$	−283.7	−5.22
32	$2Ni_3Al + 7Al \rightarrow 3Ni_2Al_3$	−585.3	−4.82
33	$Ni_3Al + 8Al \rightarrow 3NiAl_3$	−254.4	−1.82
34	$2Ni_3Al + 25Al \rightarrow 3Ni_2Al_9$	−568.8	−1.90
35	$Ni_5Al_3 + 2Al \rightarrow 5NiAl$	−203.0	−2.82
36	$3Ni_5Al_3 + 11Al \rightarrow 5Ni_3Al_4$	−830.5	−3.05
37	$2Ni_5Al_3 + 9Al \rightarrow 5Ni_2Al_3$	−583.5	−2.89
38	$Ni_5Al_3 + 12Al \rightarrow 5NiAl_3$	−228.0	−1.31

(*continued on next page*)

https://doi.org/10.1016/j.heliyon.2019.e01267

Table 2. (*Continued*)

№	Reaction	$\Delta_r H^0_{298}$, kJ/mol	$\Delta_r H^0_{298}/vV$, kJ/cm^3
39	$2Ni_5Al_3 + 39Al \rightarrow 5Ni_2Al_9$	−556.0	−1.12
40	$3NiAl + Al \rightarrow Ni_3Al_4$	−44.3	−0.82
41	$2NiAl + Al \rightarrow Ni_2Al_3$	−35.5	−0.98
42	$NiAl + 2Al \rightarrow NiAl_3$	−5.0	−0.14
43	$2NiAl + 7Al \rightarrow Ni_2Al_9$	−30.0	−0.30
44	$2Ni_3Al_4 + Al \rightarrow 3Ni_2Al_3$	−17.9	−0.15
45	$Ni_3Al_4 + 5Al \rightarrow 3NiAl_3$	29.3	0.28
46	$2Ni_3Al_4 + 19Al \rightarrow 3Ni_2Al_9$	−1.4	−0.01
47	$Ni_2Al_3 + 3Al \rightarrow 2NiAl_3$	25.5	0.37
48	$Ni_2Al_3 + 6Al \rightarrow Ni_2Al_9$	5.5	0.06
49	$2NiAl_3 + 3Al \rightarrow Ni_2Al_9$	−20.0	−0.20

For each sequence values of $\Delta u(x)$ are calculated, where x is the molar fraction of aluminum or nickel, depending on the case corresponding to the stoichiometry of the compound formed in the sequence under consideration.

Then the array of points (x, $\Delta u(x)$) of each sequence by the method of least squares was approximated to function (3). As a result, two sets of curves for t internal energy density change $u(x)$ as a function of molar fraction x were obtained. These curves for cases of excess of aluminum and nickel are shown in Fig. 11a and b, respectively.

Calculations show that in the case of an infinite excess of aluminum relative to nickel (Fig. 11a) at the stage of parallel competing reactions at the first moments of time the fastest decrease in internal energy density will be achieved by nucleation of Ni_3Al_4 compound (curve 4). However, before it is fully formed, i.e. the mole fraction of the compound is achieved the formation of NiAl compound reduces $u(x)$ faster (path 5). By analogy with gas system this means that the nuclei of Ni_3Al_4 compound will dissolve, and NiAl compound will be formed. Paths 1 and 2 cannot be realized, because at the moment when the molar fraction of Ni_3Al and NiAl compounds is reached the energy density due to the formation of NiAl compound is already noticeably lower than the energy density that would result from the formation of any of these compounds. Thus path 5 is realized according to which $NiAl_3$ compound is formed after NiAl compound. As we have seen XRD studies show exactly this sequence. However neither XRD nor TEM confirms the nucleation of the first phase of Ni_3Al_4 predicted by calculations. But since this should all be manifested at the level of nuclei, it can be confirmed or denied only by forming sample cross-section and studying it by high-resolution TEM.

In the case of an infinite excess of nickel with respect to aluminum (Fig. 11b) energy density decreases most rapidly on path 5, which goes through the formation of the

https://doi.org/10.1016/j.heliyon.2019.e01267

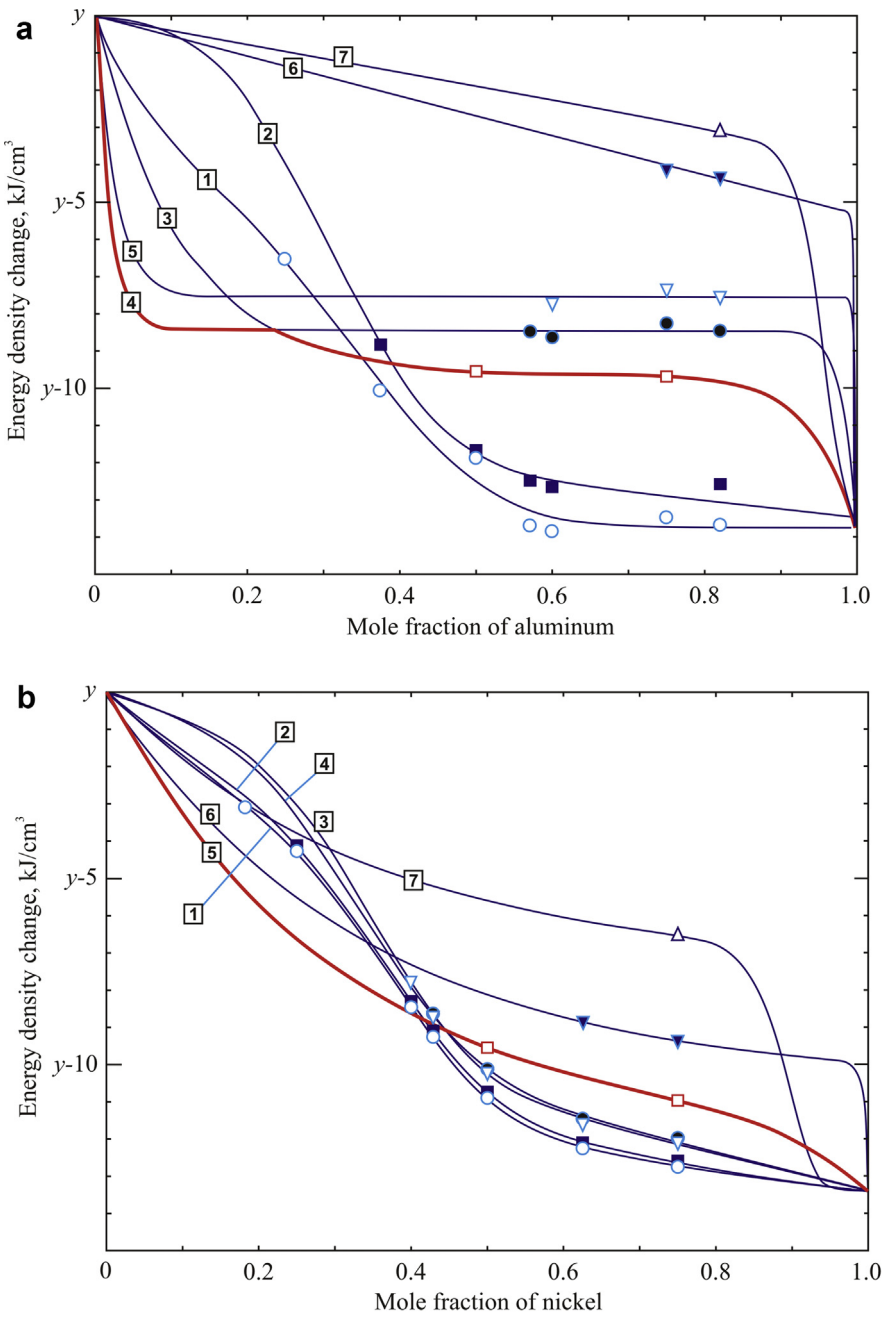

Fig. 11. The curves of energy density change in Ni-Al system as a function of mole fraction of excess element: a) case of excess of aluminum; b) case of excess of nickel. Value *y* corresponds to energy of initial state.

first NiAl compound, and then Ni_3Al compound from it. None of the other ways can be realized, because when the molar fraction of any of these compounds is reached the energy density corresponding to their formation is higher than the energy density achieved by the formation of NiAl compound. As can be seen AlNi→Ni_3Al

https://doi.org/10.1016/j.heliyon.2019.e01267

sequence is unambiguously confirmed by TEM results and, in fact, by XRD results except that after annealing at 275 °C $NiAl_3$ compound was also identified together with AlNi.

5. Conclusion

The proposed approach based on the rule of high dynamics of energy density reduction in the system quite well predicts the behavior of Ni-Al system both in the case of an aluminum excess and in the case of a nickel excess.

It should be noted that the study of a system with a large excess of one of the components including theoretical forecasts is useful, since it allows us to estimate the amount of energy that this system can emit. In particular, as can be seen from Fig. 11 for Al-Ni system both in the case of an excess of Al and in the case of an excess of Ni it is $\sim 13-14$ kJ/cm^3. Moreover, according to the calculated dynamics of the change in energy density during successive formation of compounds we can estimate the expected the rate of energy release. This is important from the viewpoint of realization of self-propagating exothermic reaction. Thus, through the proposed approach it is possible to predict new systems for SHS.

Our calculations also allow us to predict which component ratio will be optimal from the point of view of maximum heat release in the system. For the system under consideration with composition Al:Ni = 1:1, which is often used in practice and corresponds to the most stable in this system compound AlNi, the theoretical value is -9.55 kJ/cm^3. At the same time, if the compositions are 1:3 or 3:2, the expected energy value due to two successive reactions will be higher -10.97 and -10.53 kJ/cm^3, respectively.

Note also that thermodynamic method does not take into account thermal conductivity of the system, which is an important factor for SHS. Therefore, our technique is suitable for predicting the behavior of multilayer films with a greater total thickness and is less suitable for structures with a small total thickness, due to the appreciable contribution of the surface and the process of heat removal through it.

Declarations

Author contribution statement

Larisa I. Sorokina: Performed the experiments; Analyzed and interpreted the data.

Egor A. Lebedev: Conceived and designed the experiments; Performed the experiments; Analyzed and interpreted the data.

https://doi.org/10.1016/j.heliyon.2019.e01267

Alexey Yu. Trifonov: Conceived and designed the experiments; Performed the experiments; Analyzed and interpreted the data; Wrote the paper.

Dmitry G. Gromov: Conceived and designed the experiments; Analyzed and interpreted the data; Wrote the paper.

Funding statement

This work was financially supported by the Ministry of Education and Science of the Russian Federation (project No. 6.7813.2017/BY).

Competing interest statement

The authors declare no conflict of interest.

Additional information

No additional information is available for this paper.

References

[1] A.S. Edelstein, R.K. Everett, G.R. Richardson, S.B. Qadri, J.C. Foley, J.H. Perepezko, Reaction kinetics and biasing in A1/Ni multilayers, Mater. Sci. Eng. A 195 (1995) 13−19.

[2] C. Pohla, P.L. Ryder, Crystalline and quasicrystalline phases in rapidly solidified Al-Ni alloys, Acta Mater. 45 (1997) 2155−2166.

[3] H. Jones, Formation of metastable crystalline phases in light-metal systems by rapid solidification, Phil. Mag. B 61 (1990) 487−509.

[4] T.S. Dyer, Z.A. Munir, V. Ruth, The combustion synthesis of multilayer NiAl systems, Scripta Mater. 30 (1994) 1281−1286.

[5] P. Zhua, J.C.M. Lia, C.T. Liu, Reaction mechanism of combustion synthesis of NiAl, Mater. Sci. Eng. A 329−331 (2002) 57−68.

[6] A.S. Rogachev, B.P. Tolochko, N.Z. Lyakhov, M.P. Sharafutdinov, N.A. Popkov, B.Ya. Pirogov, E.B. Pis'menskaya, Characteristic features of structure formation of nickel monoaluminide formed in a gasless combustion wave, Crystallogr. Rep. 48 (2003) 466−468.

[7] D.P. Adams, Reactive multilayers fabricated by vapor deposition: a critical review, Thin Solid Films 576 (2015) 98−128.

https://doi.org/10.1016/j.heliyon.2019.e01267

[8] F. Baras, V. Turlo, O. Politano, S.G. Vadchenko, A.S. Rogachev, A.S. Mukasyan, SHS in Ni/Al nanofoils: a review of experiments and molecular dynamics simulations, Adv. Eng. Mater. 20 (2018) 1800091.

[9] S. Kanetsuki, K. Kuwahara, S. Egawa, S. Miyake, T. Namazu, Effect of thickening outermost layers in Al/Ni multilayer film on thermal resistance of reactively bonded solder joints, Jpn. J. Appl. Phys. 56 (2017) 06GN16.

[10] A. Zhang, Z. Zhou, W. Zhu, L. Mo, F. Wu, Si/Si bonding based on self-propagating exothermic reaction, 17th International Conference on Electronic Packaging Technology, ICEPT 2016 (2016) 1180−1184, 7583334.

[11] J. Braeuer, J. Besser, M. Wiemer, T. Gessner, A novel technique for MEMS packaging: reactive bonding with integrated material systems, Sens. Actuators A 188 (2012) 212−219.

[12] J. Braeuer, T. Gessner, A hermetic and room-temperature wafer bonding technique based on integrated reactive multilayer systems, J. Micromech. Microeng. 24 (2014) 115002.

[13] S. Simoes, F. Viana, M. Kocak, A.S. Ramos, M.T. Vieira, M.F. Vieira, Microstructure of reaction zone formed during diffusion bonding of TiAl with Ni/Al multilayer, J. Mater. Eng. Perform. 21 (2012) 678−682.

[14] W. Zhu, F. Wu, B. Wang, E. Hou, P. Wang, C. Liu, W. Xia, Microstructural and mechanical integrity of Cu/Cu interconnects formed by self-propagating exothermic reaction methods, Microelectron. Eng. 128 (2014) 24−30.

[15] M.R. Locatelli, B.J. Dalgleish, K. Nakashima, A.P. Tomsia, A.M. Glaeser, New approaches to joining ceramics for high-temperature applications, Ceram. Int. 23 (1997) 313−322.

[16] Z. Long, B. Dai, S. Tan, Y. Wang, X. Wei, Transient liquid phase bonding of copper and ceramic Al_2O_3 by Al/Ni nano multilayers, Ceram. Int. 43 (2017) 17000−17004.

[17] M.H. da Silva Bassani, J.H. Perepezko, A.S. Edelstein, R.K. Everett, Phase selection and sequence of phase formation in Al/Ni multilayers, Mater. Sci. Forum 225−227 (1996) 135−140.

[18] E. Ma, M.-A. Nicolet, M. Nathan, $NiAl_3$ formation in Al/Ni thin-film bilayers with and without contamination, J. Appl. Phys. 65 (1989) 2703−2710.

[19] J.C. Trenkle, L.J. Koerner, M.W. Tate, S.M. Gruner, T.P. Weihs, T.C. Hufnagel, Phase transformations during rapid heating of Al/Ni multilayer foils, Appl. Phys. Lett. 93 (2008) 081903.

https://doi.org/10.1016/j.heliyon.2019.e01267

[20] A.S. Edelstein, R.K. Everett, G.Y. Richardson, S.B. Qadri, E.I. Altman, J.C. Foley, J.H. Perepezko, Intermetallic phase formation during annealing of Al/Ni multilayers, J. Appl. Phys. 65 (1994) 7850−7859.

[21] R. Pretorius, R. de Reus, A.M. Vredenberg, F.W. Saris, Use of the effective heat of formation rule for predicting phase formation sequence in Al-Ni systems, Mater. Lett. 9 (1990) 494−499.

[22] J. Noro, A.S. Ramos, M.T. Vieira, Intermetallic phase formation in nanometric Ni/Al multilayer thin films, Intermetallics 16 (2008) 1061−1065.

[23] S.P. Murarka, Silicides for VLSI Applications, Academic Press, New York, 1983.

[24] F.M. d'Heurle, Nucleation of a new phase from the interaction of two adjacent phases: some silicides, J. Mater. Res. 3 (1988) 167−195.

[25] J.S. Kim, T. LaGrange, B.W. Reed, M.L. Taheri, M.R. Armstrong, W.E. King, N.D. Browning, G.H. Campbell, Imaging of transient structures using nanosecond in situ TEM, Science 321 (2008) 1472−1475.

[26] Ł. Maj, J. Morgiel, In-situ transmission electron microscopy observations of nucleation and growth of intermetallic phases during reaction of Ni(V)/Al multilayers, Thin Solid Films 621 (2017) 165−170.

[27] D. Shi, B. Wen, R. Melnik, S. Yao, T. Li, First-principles studies of Al−Ni intermetallic compounds, J. Solid State Chem. 182 (2009) 2664−2669.

[28] E.G. Moroni, G. Kresse, J. Hafner, J. Furthmüller, Ultrasoft pseudopotentials applied to magnetic Fe, Co, and Ni: from atoms to solids, Phys. Rev. B 56 (1997) 15629.

[29] C.S. Barrett, T.B. Massalski, Structure of Metals, 3rd Revised Edition, Pergamon Press, Oxford, 1980.

[30] K.J. Blobaum, D. Van Heerden, A.J. Gavens, T.P. Weihs, Al/Ni formation reactions: characterization of the metastable Al_9Ni_2 phase and analysis of its formation, Acta Mater. 51 (2003) 3871−3884.

[31] R. Saniz, L.-H. Ye, T. Shishidou, A.J. Freeman, Structural, electronic, and optical properties of $NiAl_3$: first-principles calculations, Phys. Rev. B 74 (2006) 014209.

[32] A. Pasturel, C. Colinet, A.T. Paxton, M. van Schilfgaarde, First-principles determination of the Ni-Al phase diagram, J. Phys. Condens. Matter 4 (1992) 945−959.

[33] A.J. Bradley, A. Taylor, Xcix. The crystal structures of Ni_2Al_3 and $NiAl_3$, the London, Edinburgh, and Dublin, Phil. Mag. J. Sci. 23 (158) (1937) 1049−1067.

https://doi.org/10.1016/j.heliyon.2019.e01267

[34] R. Hultgren, Select Values of the Thermodynamic Properties of Binary Alloys, American Society for Metals, Metals Park, Ohio, 1973.

[35] O. Kubaschewski, C.B. Alcock, Metallurgical Thermochemistry, Pergamon Press, Oxford, 1983.

[36] F.R. de Boer, R. Boom, V.C.M. Mattens, A.R. Miedema, A.K. Niessen, Cohesion in metals: transition metal alloys, in: F.R. de Boer, D. Pettifor (Eds.), Cohesion and Structure, Elsevier, North Holland, Amsterdam, 1988.

[37] C. Michaelsendag, K. Barmakddagand, T.P. Weihs, Investigating the thermodynamics and kinetics of thin film reactions by differential scanning calorimetry, J. Phys. D Appl. Phys. 30 (1997) 3167−3186.

[38] Von R. Hultgren, R.L. Orr, P.D. Anderson, K.K. Kelley, Selected Values of Thermodynamic Properties of Metals and Alloys, John Wiley & Sons, New York-London, 1963.

[39] I. Ansara, B. Sundman, P. Willemin, Thermodynamic modeling of ordered phases in the Ni-Al system, Acta Metall. 36 (1988) 977−982.

[40] R.E. Watson, M. Weinert, Transition-metal aluminide formation: Ti, V, Fe, and Ni aluminides, Phys. Rev. B 58 (1998) 5981.

[41] P.D. Desai, Thermodynamic properties of selected binary aluminum alloy systems, J. Phys. Chem. Ref. Data 16 (1987) 109−124.

[42] J.E. Garcés, G. Bozzolo, Determination of structural alloy equilibrium properties from quantum approximate methods, Phys. Rev. B 71 (2005) 134201.

[43] W. Lin, A.J. Freeman, Cohesive properties and electronic structure of Heusler $L2_1$-phase compounds Ni_2XAl (X=Ti, V, Zr, Nb, Hf, and Ta), Phys. Rev. B 45 (1992) 61.

[44] V.V. Samokhval, A.A. Vecher, E.P. Pan'ko, Thermodynamic properties of AlSb and AlSb-GaSb solid solutions, in: N.N. Sirota (Ed.), Chemical Bonds in Solids, Springer, Boston, 1972, pp. 184−187.

[45] B.I. Min, T. Oguchi, H.J.F. Jansen, A.J. Freeman, Structural, electronic and magnetic properties of NiAl and FeAl alloys, J. Magn. Magn Mater. 54−57 (1986) 1091−1092.

[46] B.P. Burton, J.E. Osburn, A. Pasturel, LMTO/CVM and LAPW/CVM Calculations of the NiAl-NiTi Pseudobinary Phase Diagram, MRS Online Proc. Libr. 213 (1990). Symposium Q − High-Temperature Ordered Intermetallic Alloys IV.

https://doi.org/10.1016/j.heliyon.2019.e01267

[47] Z.W. Lu, S.-H. Wei, A. Zunger, S. Frota-Pessoa, L.G. Ferreira, First-principles statistical mechanics of structural stability of intermetallic compounds, Phys. Rev. B 44 (1991) 512.

[48] W. Lin, J. Xu, A.J. Freeman, Cohesive properties, electronic structure, and bonding characteristics of RuAl - a comparison to NiAl, J. Mater. Res. 7 (1992) 592−604.

[49] B.P. Burton, J.E. Osburn, A. Pasturel, Theoretical calculations of the NiAl-NiTi phase diagram based on first-principles linear-muffin-tin-orbital and full-potential linearly-augmented plane-wave cohesive-energy calculations, Phys. Rev. B 45 (1992) 7677.

[50] P.A. Schultz, J.W. Davenport, Bonding and brittleness in B2 structure 3*d* transition metal aluminides: ionic, directional, or does it make a difference? Scripta Metall. Mater. 27 (1992) 629−634.

[51] K. Rzyman, Z. Moser, R.E. Watson, M. Weinert, Enthalpies of formation of AlNi: experiment versus theory, J. Phase Equil. 19 (1998) 106−111.

[52] D.H. Dieter, L.H. Leo, Calorimetric determination of the enthalpies of formation of some intermetallic compounds, Z. Metallkd./Mater. Res. Adv. Techn. 65 (1974) 642−649.

[53] S.V. Meschel, O.J. Kleppa, The standard enthalpies of formation of some 3d transition metal aluminides by high-temperature direct synthesis calorimetry, in: J.S. Faulkner, R.G. Jordan (Eds.), Metallic Alloys: Experimental and Theoretical Perspectives, NATO ASI Series, Springer, Heidelberg, 1994, pp. 103−112.

[54] R. Hu, P. Nash, The enthalpy of formation of NiAl, J. Mater. Sci. 40 (2005) 1067−1069.

[55] P. Nash, O. Kleppa, Composition dependence of the enthalpies of formation of NiAl, J. Alloy. Comp. 321 (2001) 228−231.

[56] A.K. Niessen, A.R. Miedema, F.R. de Boer, R. Boom, Enthalpies of formation of liquid and solid binary alloys based on 3d metals: IV. Alloys of cobalt, Phys. B+C 151 (1988) 401−432.

[57] P. Villars, L.D. Calvert, Pearson's Handbook of Crystallographic Data for Intermetallic Phases, American Society for Metals, Metals Park, Ohio, 1986.

[58] M.C. Payne, M.P. Teter, D.C. Allan, T.A. Arias, J.D. Joannopoulos, Iterative minimization techniques for ab initio total-energy calculations: molecular dynamics and conjugate gradients, Rev. Mod. Phys. 64 (1992) 1045−1097.

[59] D.R. Hamann, M. Schlüter, C. Chiang, Norm-conserving pseudopotentials, Phys. Rev. Lett. 43 (1979) 1494−1497.

https://doi.org/10.1016/j.heliyon.2019.e01267